ISSN 1063-7761, Journal of Experimental and Theoretical Physics, 2014, Vol. 119, No. 4, pp. 737–744. © Pleiades Publishing, Inc., 2014.
Original Russian Text © A.A. Demidov, D.V. Volkov, I.A. Gudim, E.V. Eremin, K.N. Boldyrev, 2014, published in Zhurnal Eksperimental'noi i Teoreticheskoi Fiziki, 2014, Vol. 146, No. 4, pp. 835–843.

ORDER, DISORDER, AND PHASE TRANSITION IN CONDENSED SYSTEM

Magnetic, Magnetoelastic, and Spectroscopic Properties of $TmAl_3(BO_3)_4$

A. A. Demidov[a], D. V. Volkov[b], I. A. Gudim[c], E. V. Eremin[c], and K. N. Boldyrev[d]

[a] *Bryansk State Technical University, Bryansk, 241035 Russia*
[b] *Moscow State University, Moscow, 119992 Russia*
[c] *Kirensky Institute of Physics, Siberian Branch, Russian Academy of Sciences, Krasnoyarsk, 660036 Russia*
[d] *Institute of Spectroscopy, Russian Academy of Sciences, Troitsk, Moscow, 142190 Russia*
e-mail: demandr@yandex.ru

Received April 25, 2014

Abstract—The thermodynamic properties of alumoborate $TmAl_3(BO_3)_4$ single crystal are studied experimentally and theoretically. A theoretical analysis based on the crystal field model makes it possible to interpret all measured parameters. The crystal field parameters are determined. The temperature (3–300 K) and field (up to 9 T) dependences of magnetization are described. The field and temperature dependences of multipole moments of the Tm^{3+} ion in $TmAl_3(BO_3)_4$ make it possible to describe magnetostriction and low-temperature anomalies in thermal expansion.

DOI: 10.1134/S106377611410015X

1. INTRODUCTION

The rare-earth borates $RM_3(BO_3)_4$ (R = Y, La–Lu; M = Fe, Al, Cr, Ga), which have been intensely studied in recent years, have a trigonal structure and possess magnetoelectric properties important for applications (see, for example, [1–6] and review [7]). It has been found that borates with two magnetic subsystems (ferroborates $RFe_3(BO_3)_4$) belong to multoferroics [1, 4, 7]; the quantum theory of their magnetoelectricity has been recently formulated [8]. Borates with a single magnetic subsystem (alumoborates $RAl_3(BO_3)_4$) combine luminescent and clearly manifested nonlinear optical properties; it has been established recently that these materials are characterized by their striking magnetoelectric properties [9–12].

The growing interest in borates $RM_3(BO_3)_4$ is due to the discovery of the record-high magnetoelectric polarization for multiferroics in $HoAl_3(BO_3)_4$, which amounts to $\Delta P_{ab}(B_b) \approx -3600$ μC/m^2 in a field of 7 T at $T = 3$ K [10] and is several times higher than the maximal values of polarization (including that in ferroborates). It was found in [12] that the polarization of $HoAl_3(BO_3)_4$ attains a much higher value ($\Delta P_{ba}(B_a) \approx -5240$ μC/m^2) in field $B = 9$ T at $T = 5$ K. A strong magnetoelectric effect (about 750 μC/m^2) was also observed in alumoborate $TmAl_3(BO_3)_4$ [9, 11].

The magnetostriction of alumoborates with R = Tm and Ho and thermal expansion for R = Tm were investigated experimentally in [9, 10]. The magnetostriction, deformation susceptibility, and thermal expansion curves for ferroborates $RFe_3(BO_3)_4$ with R = Nd, Tb, Pr, and Dy [13–16] and alumoborate $HoAl_3(BO_3)_4$ [17] were calculated earlier using the approach developed in [18, 19] and implemented in [13] for the case of trigonal symmetry; these studies have made it possible to describe the striking anomalies in magnetoelastic properties that have been experimentally observed and to predict a number of effects.

This study is aimed at an analysis of the thermodynamic properties of alumoborate $TmAl_3(BO_3)_4$, a comparison of experimental data with the results of calculations, and the determination of the parameters of this compound.

2. EXPERIMENT

$TmAl_3(BO_3)_4$ single crystals were grown from solution–melts based on bismuth trimolybdate and lithium molybdate [20] 85% by mass [$Bi_2Mo_3O_{12} + 2B_2O_3 + 0.4Li_2MoO_4$] + 15% by mass $TmAl_3(BO_3)_4$ in accordance with the technique described in detail in [21]. The magnetic properties were studied using a PPMS-9 (Quantum Design) in the temperature range 3–300 K in magnetic fields up to 9 T. The absorption spectra were recorded in wide temperature (3.2–300 K) and spectral (2000–25000 cm^{-1}) ranges on a Bruker IFS 125HR Fourier spectrometer with a spectral resolution of 0.1 cm^{-1}. Data on the order of energy levels of the ground state were obtained by recording the absorption spectra of linearly polarized light in the geometries $\mathbf{k} \perp \mathbf{c}$, $\mathbf{E} \perp \mathbf{c}$ (σ polarization) and $\mathbf{k} \perp \mathbf{c}$, $\mathbf{E} \parallel \mathbf{c}$ (π polarization).

3. COMPUTATIONAL TECHNIQUE

In our calculations, we used the results of analysis of compounds $HoAl_3(BO_3)_4$ [12, 17], galloborate $HoGa_3(BO_3)_4$ [5], ferroborates $RFe(BO_3)_4$ [2, 13–16], which are isostructural to alumoborate $TmAl_3(BO_3)_4$, as well as garnets $R_3Al_5O_{12}$ and $R_3Ga_5O_{12}$ [18] and zircons RXO_4 (X = P, V) [19, 22].

For calculating the magnetic and magnetoelastic characteristics and the Zeeman effect, we used Hamiltonian $\mathcal{H}$ including the crystal field (CF) Hamiltonian $\mathcal{H}_{CF}$, Zeeman term $\mathcal{H}_Z$, and magnetoelastic Hamiltonian $\mathcal{H}_{ME}$ written in the multipole approximation

$$\mathcal{H} = \mathcal{H}_{CF} + \mathcal{H}_Z + \mathcal{H}_{ME}, \quad (1)$$

$$\mathcal{H}_{CF} = B_0^2 C_0^{(2)} + B_0^4 C_0^{(4)} + iB_{-3}^4 (C_{-3}^{(4)} + C_3^{(4)}) + B_0^6 C_0^{(6)} + iB_{-3}^6 (C_{-3}^{(6)} + C_3^{(6)}) + B_6^6 (C_{-6}^{(6)} + C_6^{(6)}), \quad (2)$$

$$\mathcal{H}_Z = -g_J \mu_B \mathbf{B} \cdot \mathbf{J}. \quad (3)$$

The CF Hamiltonian with the symmetry D_3 is written for the case when the c is the trigonal axis and a is the twofold axis. In these expressions, B_q^k are the CF parameters, $C_q^{(k)}$ are irreducible tensor operators, g_J is the Lande factor, and **J** is the angular momentum operator for the rare-earth ion.

The magnetization of paramagnetic $TmAl_3(BO_3)_4$ in external field **B** is given by

$$\mathbf{M} = g_J \mu_B \langle \mathbf{J} \rangle. \quad (4)$$

The magnetoelastic Hamiltonian $\mathcal{H}_{ME}$ of the rare-earth subsystem for a crystal of the trigonal symmetry was written earlier in [13] taking into account fourth-order operators. It was shown in [13] that the expressions for magnetostriction have the form of linear combinations of the multipole moments of the R ion. The coefficients are the combinations of the corresponding magnetoelastic coefficients and elastic compliances, determined by symmetry. Let us write the expressions for longitudinal (5) and transverse (6) magnetostrictions required to interpret the magnetostriction of $TmAl_3(BO_3)_4$ in the field directed along the a axis, where these combinations are denoted by A, B, C, D, etc., (see [13] for details):

$$\left[\frac{\Delta l}{l}\right]_{[100]}^{[100]} = \left.\frac{\Delta a}{a}\right|_{\mathbf{B} \parallel \mathbf{a}} = \Delta\{A_a \alpha_J \langle O_2^0 \rangle + B_a \beta_J \langle O_4^0 \rangle + C_a \beta_J \langle \Omega_4^3 \rangle + D\alpha_J \langle \Omega_2^1 \rangle + E\alpha_J \langle O_2^2 \rangle + F\beta_J \langle \Omega_4^1 \rangle + G\beta_J \langle O_4^2 \rangle + H\beta_J \langle O_4^4 \rangle\}, \quad (5)$$

$$\left[\frac{\Delta l}{l}\right]_{[100]}^{[001]} = \left.\frac{\Delta c}{c}\right|_{\mathbf{B} \parallel \mathbf{a}} = \Delta\{A_c \alpha_J \langle O_2^0 \rangle + B_c \beta_J \langle O_4^0 \rangle + C_c \beta_J \langle \Omega_4^3 \rangle\}. \quad (6)$$

In these expressions the superscript and subscript on $[\Delta l/l]$ are the unit vectors for the direction of measurement of magnetostriction and magnetic field direction, respectively; α_J and β_J are the Stevens coefficients, and $\langle O_n^m \rangle$ and $\langle \Omega_n^m \rangle$ are the thermal mean values of the corresponding equivalent operators, calculated on the energy spectrum and wavefunctions of the R ion, which are formed by the crystal field and external field **B**. The calculation of these thermal mean values makes it possible to find out which of these characteristics determine the field and temperature dependences of the magnetostriction.

The magnetoelastic contribution to thermal expansion can also be calculated using the above expressions (5) and (6), which are used for determining the temperature variations of multipole moments of the rare-earth ion in zero external field.

4. RESULTS AND DISCUSSION

The crystal field, which determines to a considerable extent the electron structure of rare-earth ions (their energy spectrum and wavefunctions), plays the most important role in the formation of the physical properties of rare-earth compounds. At low temperatures, a considerable contribution also comes from the magnetoelastic interaction associated with the change in asphericity of the $4f$ shell of the R ion upon a change in external parameters (temperature, magnetic field, and so on). Magnetoelastic phenomena (magnetostriction, anomalies in lattice parameters and elastic constants) strongly depend on the R ion and the symmetry of its surroundings. To obtain a correct description of magnetic and magnetoelastic properties, it is necessary to use a reliable set of the CF parameters B_q^k in calculations; for this reason, the description of properties of $TmAl_3(BO_3)_4$ should begin with the determination of the CF parameters.

In the search for the CF parameters, we took into account spectroscopic information and the CF parameters from [23] determined for $YAl_3(BO_3)_4$:Tm^{3+}. Although alumoborate $YAl_3(BO_3)_4$:Tm^{3+} and not $TmAl_3(BO_3)_4$ was studied in [23], the energy level diagrams (order of doublets and singlets as well as their numbers) should not differ significantly for these two compounds; the values of specific splitting between the levels can be different. The calculations with the CF parameters for $YAl_3(BO_3)_4$:Tm^{3+} from [23] and their comparison with the magnetic characteristics measured in our experiments show a substantial difference between the resultant anisotropy of magnetization and the experimental value. The magnetization curve $M_c(B)$ calculated for the field direction $\mathbf{B} \parallel \mathbf{c}$ and temperature dependences $M_c(T)$ for $B = 0.1$–9.0 T are found to be much lower than the experimental curves. For the field directed in the basal plane, the calculated $M_{\perp c}(B)$ and

$M_{\perp c}(T)$ curves are close to the experimental dependences.

Analysis of the transmission spectra measured for $TmAl_3(BO_3)_4$ has made it possible to identify the following values of energy of the ground multiplet of the Tm^{3+} ion (d doublet): 0, 27^d, 100^d, 197, 256, 290, 315, 363^d, and 458^d cm^{-1}. It should be noted that the resultant energy values are in conformity with the data obtained for the Tm^{3+} ion in $YAl_3(BO_3)_4$:Tm^{3+} in [23], where only some lower levels of the ground multiplet were investigated.

To determine the CF parameters for $TmAl_3(BO_3)_4$, we used available information on the structure of the ground multiplet (energy values, order of singlets and doublets), as well as the data on magnetization curves $M_{c,\perp c}(B)$ recorded at $T = 3$ K in fields up to 9 T and on the temperature dependences of magnetization $M_{c,\perp c}(T)$ obtained in the temperature range from 3 K to 300 K for $B = 0.1$ and 9 T. As the initial values of the CF parameters, we used the parameters for $YAl_3(BO_3)_4$:Tm^{3+} [23], $TbAl_3(BO_3)_4$ [24], $HoAl_3(BO_3)_4$ [17], and $HoGa_3(BO_3)_4$ [5]. Following the criteria of description of the $M_{c,\perp c}(B)$ and $M_{c,\perp c}(T)$ dependences and reproduction of the structure of the ground multiplet, we chose the following set of the CF parameters, which made it possible to correctly describe the entire body of experimental data (B_q^k, in cm^{-1}):

$$B_0^2 = 561, \quad B_0^4 = -938, \quad B_{-3}^4 = -475,$$
$$B_0^6 = 540, \quad B_{-3}^6 = -137, \quad B_6^6 = 575. \qquad (7)$$

Since these parameters were determined in calculations on the basis of the ground multiplet, they can be treated as suitable for describing thermodynamic properties.

Set of parameters (7) corresponds to the following energy values for 13 lower Stark levels of the ground multiplet of the Tm^{3+} ion in $TmAl_3(BO_3)_4$ ($B = 0$): 0, 27^d, 93.6^d, 148, 252.5, 293, 301, 385^d, and 497^d cm^{-1}. The resultant energy level diagram for the ground multiplet exactly reproduces the experimentally determined diagram and is close to the experimental values of energy.

Figure 1 shows that with increasing field, the $M_{c,\perp c}(B)$ curves obtained at $T = 3$ K demonstrate strong anisotropy. The calculated magnetization curves with parameters (7) correctly describe the corresponding experimental curves recorded at $T = 3$ and 295 K. The Zeeman effect corresponding to the calculated $M_{c,\perp c}(B)$ dependences at $T = 3$ K is shown in the inset to Fig. 1. The stronger splitting of the lower energy levels for the Tm^{3+} ion with $\mathbf{B} \perp \mathbf{c}$ as compared to $\mathbf{B} \parallel \mathbf{c}$ determines the observed behavior of the $M_{c,\perp c}(B)$ curves.

It can be seen from Fig. 1 that the $M_c(B)$ curve obtained at $T = 295$ K lies higher than the curve obtained at $T = 3$ K, although the magnetization of the paramagnetic compounds usually decreases with an increase in temperature. This can be explained by the large spacing between the lower energy levels of the ground multiplet of the Tm^{3+} ion in $TmAl_3(BO_3)_4$ and by their small splitting in field $\mathbf{B} \parallel \mathbf{c}$ (see the inset to Fig. 1). As a result, the levels that do not participate in magnetization at low temperatures make a contribution to the magnetization $M_c(B)$ of the compound at high temperatures.

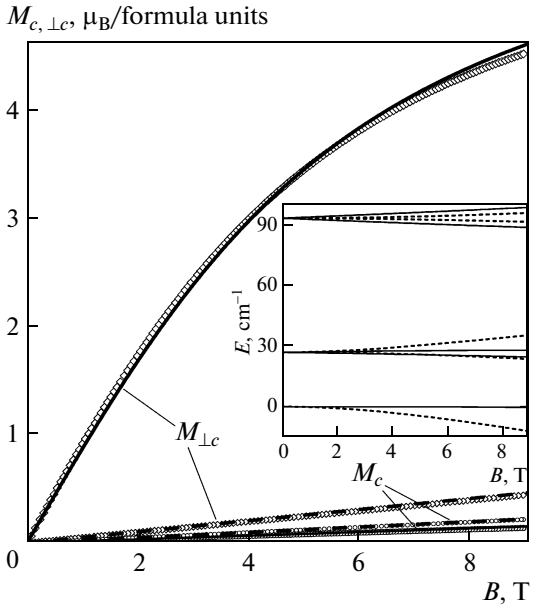

Fig. 1. Magnetization curves for $TmAl_3(BO_3)_4$ in field $\mathbf{B} \parallel \mathbf{c}$ and $\mathbf{B} \perp \mathbf{c}$ at $T = 3$ K (solid curves) and $T = 295$ K (dashed curves). Symbols are experimental data and curves are results of calculation. Inset shows the Zeeman effect at $T = 3$ K; five lower energy levels of the ground multiplet of the Tm^{3+} ion are given for $\mathbf{B} \parallel \mathbf{c}$ (solid curves) and $\mathbf{B} \perp \mathbf{c}$ (dashed curves).

It should be noted that we also calculated the Zeeman effect in strong fields (up to 200 T) for $\mathbf{B} \parallel \mathbf{c}$, $\mathbf{B} \perp \mathbf{c}$ to analyze the possible effects associated with the interaction (crossover) of energy levels of the Tm^{3+} ion in a magnetic field, which provide valuable information on the crystal field. In paramagnetic compounds with the structure of zircon RXO_4 (X = P, V), crossovers are observed almost for all R and are accompanied by striking magnetic anomalies in the magnetic characteristics (see, for example, [25, 26]). Analogous effects in moderate and strong magnetic fields are also expected in alumoborates $RAl_3(BO_3)_4$. Calculations show that the crossover is observed in $TmAl_3(BO_3)_4$ for $\mathbf{B} \parallel \mathbf{c}$ and $T = 4.2$ K near 90 T; as a result, a large (about $5\mu_B$) jump is observed on the $M_c(B)$ curve as well as the corresponding maximum of the differential magnetic susceptibility dM_c/dB. The sizes of the field in which the crossovers occur strongly depend on the specific CF parameters and can serve as indicators for their refinement.

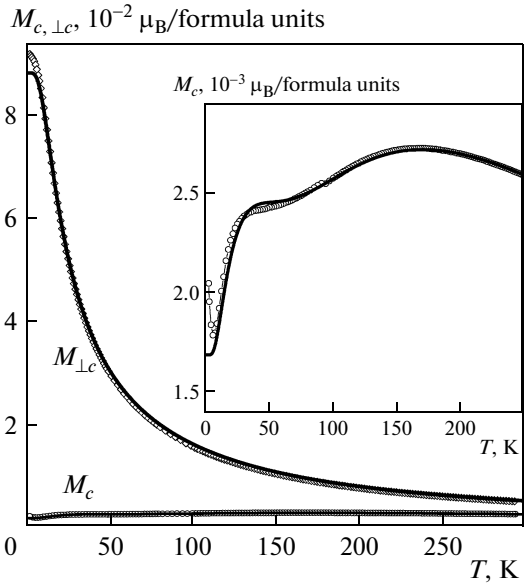

Fig. 2. Temperature dependences of magnetization $M_{c,\perp c}$ of $TmAl_3(BO_3)_4$ for $B = 0.1$ T. Symbols are experimental data and curves are results of calculation. Inset shows $M_c(T)$ curves on a magnified scale.

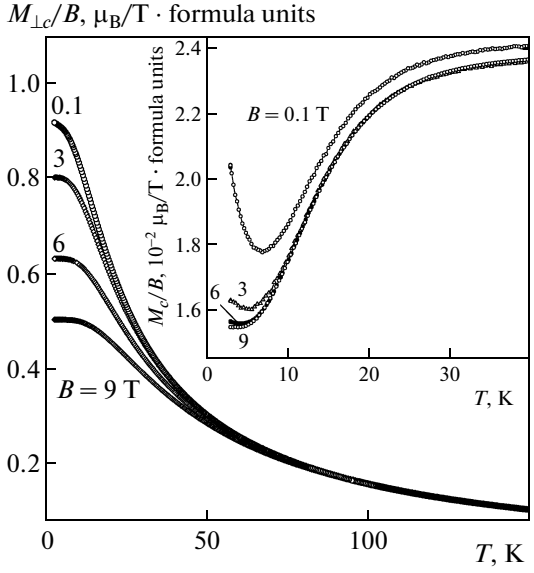

Fig. 3. Experimental temperature dependences of $M_{\perp c}/B$ and M_c/B (low-temperature region is shown in the inset) for $TmAl_3(BO_3)_4$ for various field values.

Figure 2 shows the temperature dependences of magnetization $M_{c,\perp c}(T)$ for $B = 0.1$ T, which can be interpreted as the susceptibility. It can be seen that the calculated curves correctly describe the experimental dependences. The resulting CF parameters make it possible to reproduce a Schottky-type anomaly near $T = 30$ K on the experimental $M_c(T)$ dependence (see the inset to Fig. 2), which is associated with the redistribution of the populations of the lower states of the Tm^{3+} ion. The $M_c(T)$ curve calculated for the lowest temperatures tends to a constant value in contrast to the experimental curve on which the low-temperature increase is observed (see the inset to Fig. 2). This difference is due to the possible presence of paramagnetic impurities in the sample.

It should be noted that the susceptibility $\chi_{a,c}(T)$ curves of $TmAl_3(BO_3)_4$ were measured earlier in [9, 11]. It is interesting that comparison of the $\chi_c(T)$ curve from [9, 11] with the $M_c(T)$ curve measured in this study shows a significant difference in the low-temperature region (at $T < 50$ K). The $\chi_c(T)$ curve from [9, 11] increases upon a decrease in temperature, while the $M_c(T)$ dependence measured at $B = 0.1$ T (and for larger values of B) decreases upon cooling. Calculations performed with different CF parameters show a decrease in susceptibility with the temperatures at $T <$ 50 K. We can conjecture that during measurement of the $\chi_c(T)$ curve in [9, 11], a disorientation took place, as a result of which the additional component of the susceptibility in the basal plane considerably increased the measured value of $\chi_c(T)$.

The experimental $M_{c,\perp c}/B(T)$ curves shown in Fig. 3, which were measured for $B = 0.1$, 3, 6, and 9 T, make it possible to explain how the behavior of the temperature dependence of the magnetization in field B changes depending on the applied field. It can be seen that for the direction **B** || **c** (inset to Fig. 3), the low-temperature anomaly becomes less pronounced with an increasing field and disappears for $B > 6$ T. The shape and the position of the Schottky anomaly near $T = 30$ K, which is determined by splitting (near 27 cm^{-1}) between the lower energy levels of the Tm^{3+} ion, is independent on the magnitude of applied field B.

The experimental and calculated $M_{c,\perp c}(T)$ dependences shown in Fig. 4 for $B = 3$, 6, and 9 T indicate that all features of the experimental curves can be described successfully in the entire temperature range. It should be noted that the $M_c(T)$ dependences obtained for $B = 3$–9 T demonstrate the increase in magnetization $M_c(T)$ with temperature, which was observed in the analysis of the magnetization curves $M_c(B)$ obtained at $T = 3$ K and 295 K (see Fig. 1).

The field and temperature dependences of multipole moments of the Ho^{3+} ion in $HoAl_3(BO_3)_4$ calculated earlier in [17] have made it possible to describe magnetostriction from [10] and to predict thermal expansion anomalies. We performed analogous calculations for $TmAl_3(BO_3)_4$.

The longitudinal and transverse magnetostriction in $TmAl_3(BO_3)_4$ for field direction **B** || **a** was measured in [9] in the temperature interval from 3 to 100 K in fields up to 7 T. The experimental curves for the longitudinal magnetization [9] at **B** || **a** and $T = 3$–100 K shown in Fig. 5a are nonlinear. It can be seen that the field directed along the a axis leads to a compression of the crystal in the direction of the a axis. Figure 5b

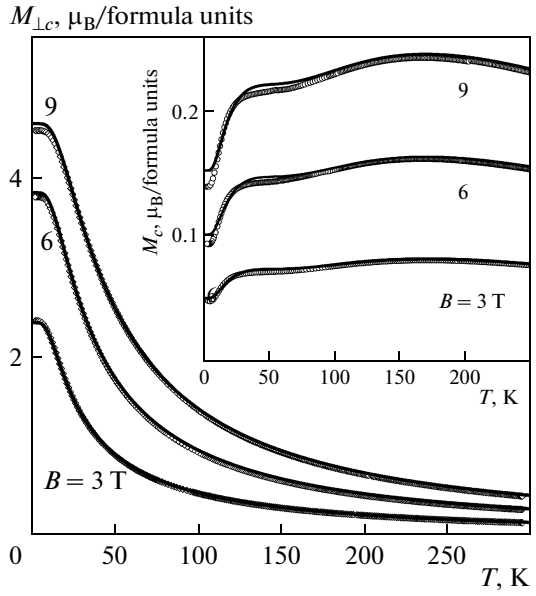

Fig. 4. Temperature dependences of magnetizations $M_{\perp c}$ and M_c (inset) of $TmAl_3(BO_3)_4$ for various field values. Symbols are experimental data and curves are results of calculation.

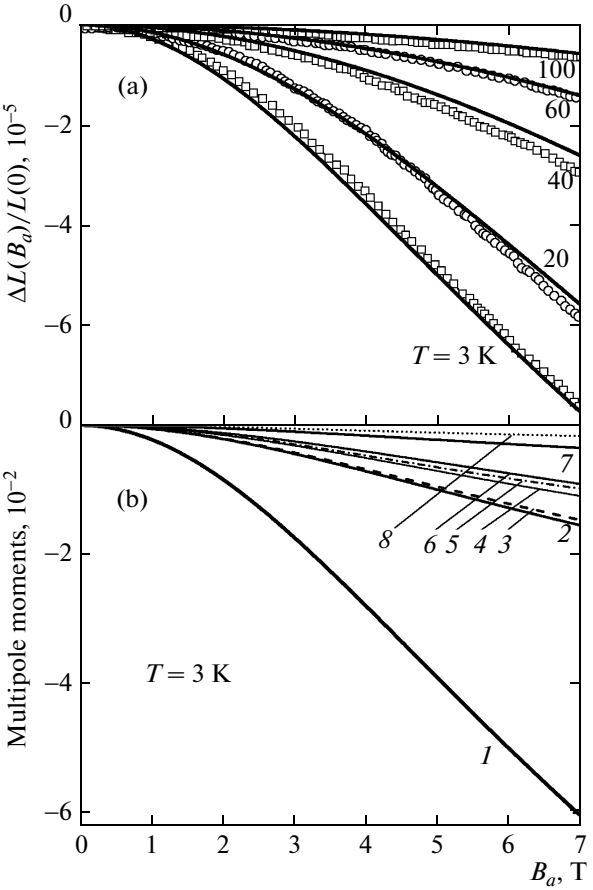

Fig. 5. Experimental (symbols) field dependences of the longitudinal magnetostriction of $TmAl_3(BO_3)_4$ [9] along a axis of the crystal and calculated (curves) field dependences of multipole moments of Tm^{3+} ion in $TmAl_3(BO_3)_4$ for $\mathbf{B} \parallel \mathbf{a}$. (a) $T = 3$–100 K, $E\alpha_J\langle O_2^2\rangle$; (b) $T = 3$ K, $-\alpha_J\langle O_2^2\rangle$ (*1*), $-\beta_J\langle O_4^2\rangle$ (*2*), $-\beta_J\langle \Omega_4^1\rangle$ (*3*), $-\alpha_J\langle \Omega_2^1\rangle$ (*4*), $\beta_J\langle \Omega_4^4\rangle$ (*5*), $-\beta_J\langle \Omega_4^0\rangle$ (*6*), $-\alpha_J\langle \Omega_2^0\rangle$ (*7*), and $-\beta_J\langle \Omega_4^3\rangle$ (*8*).

shows the field dependences of multipole moments appearing in formula (5) for field lying in the basal plane ($\mathbf{B} \parallel \mathbf{a}$) at $T = 3$ K. By multipole moments, we mean their variations in the field

$$\begin{aligned} \langle O_n^m\rangle &= \langle O_n^m\rangle_B - \langle O_n^m\rangle_{B=0}, \\ \langle \Omega_n^m\rangle &= \langle \Omega_n^m\rangle_B - \langle \Omega_n^m\rangle_{B=0}. \end{aligned} \tag{8}$$

Comparison of the field dependences of all multipole moments in Fig. 5b shows that moment $\alpha_J\langle O_2^2\rangle$ (curve *1*) increases with the field more strongly than other moments. The behavior of this moment completely matches the experimental field dependence of magnetostriction for $\mathbf{B} \parallel \mathbf{a}$ at $T = 3$ K (see Fig. 5a). This enabled us to estimate coefficient E (see formula (5)) from a comparison of the experimental and calculated curves, taking into account the fact that the remaining multipole moments behave analogously. Coefficient E, as well as other coefficients in formulas (5) and (6), is a combination of the magnetoelastic coefficients B_{nm}^{μ} and elastic constants C_0^{ν} (see notation in [13]). It has the form

$$E = \frac{B_{22}^{\varepsilon}C_0^{\xi} - B_{22}^{\xi}C_0^{\varepsilon\xi}}{\sqrt{2}(C_0^{\varepsilon}C_0^{\xi} - (C_0^{\varepsilon\xi})^2)}. \tag{9}$$

Its value is $E = -1.28 \times 10^{-3}$. Calculations of the field dependences of actual moment $\alpha_J\langle O_2^2\rangle$ for high temperatures at which the magnetostriction was measured show good general agreement with experiment (see Fig. 5a). According to the results of calculations, all remaining multipole moments remain smaller at all temperatures. It should be noted that according to [17], the largest multipole moment responsible for the behavior of magnetostriction in $HoAl_3(BO_3)_4$ with the field lying in the basal plane is also moment $\alpha_J\langle O_2^2\rangle$ (and $\beta_J\langle O_4^2\rangle$ to a certain extent).

We attempted to describe the magnetostriction curves obtained [9] along the **c** axis for $\mathbf{B} \parallel \mathbf{a}$. In the results for transverse magnetostriction, the curves obtained at $T = 3$ K differ considerably for those at $T = 5$ K. For example, in a field of 7 T, the transverse magnetostriction at $T = 3$ K is approximately 1.7 times higher than that at the close temperature $T = 5$ K (see Fig. 3b in [9]). The shape of the curve for $T = 3$ K noticeably differs from all other measured curves for

longitudinal and transverse magnetostriction for **B** || **a**. The reason for the strong difference between the values of the magnetostriction obtained at $T = 3$ K and 5 K in the compound with rare-earth ion Tm^{3+} remains unclear. We can conjecture that impurities were present in the sample and/or there were disorientation effects during measurements.

The calculation of the field dependences of multipole moments $-\alpha_J\langle O_2^0\rangle$, $-\beta_J\langle O_4^0\rangle$, and $-\beta_J\langle \Omega_4^3\rangle$ appearing in expression (6) for the magnetostriction along the trigonal axis for the field lying in the basal plane (**B** || **a**) at $T = 5$ K shows that moment $-\beta_J\langle O_4^0\rangle$ increases with the field more strongly than other moments. The behavior of this moment is in good agreement with the experimental dependence of the magnetostriction for **B** || **a** at $T = 5$ K. The transverse magnetostriction curve exhibits a substantially stronger temperature dependence than the longitudinal magnetostriction. However, the temperature dependence for moment $-\beta_J\langle O_4^0\rangle$ considered here differs from that observed in experiment. None of the multipole moments appearing in formula (6) demonstrates a temperature dependence close to that for transverse magnetostriction. We did not take into account the six-order multipole moments, for which a stronger temperature dependence cannot be excluded beforehand because the available data on low-temperature transverse magnetostriction are dubious in our opinion.

Low-temperature anomalies in the thermal expansion were detected experimentally for many rare-earth compounds (intermetallides [27], paramagnetic garnets [18, 28], zircons [22], and so on). Experimental data were described in terms of the rare-earth contribution proportional to the linear combination of multipole moments of the R ion and calculated in the first order of perturbation theory in the magnetoelastic interaction $\mathcal{H}_{\mathrm{ME}}^R$ [18, 19, 22, 28].

The temperature dependences of the multipole moments of R ions determine the temperature dependences of the lattice parameters (thermal expansion) in the low-temperature range in which the phonon contribution has already been frozen out. The possibility of observing the rare-earth contribution depends on temperature. The rare-earth contribution to the thermal expansion is determined by the energy spectrum (and wavefunctions) of the R ion, which is formed by the crystal field. It was shown in [14] that no anomalies exist at $T < T_N = 40$ K in completely symmetric multipole moments for ferroborate $TbFe_3(BO_3)_4$ isostructural to alumoborates in view of a large energy gap between the lower energy levels of the Tb^{3+} ion; accordingly thermal expansion anomalies are not expected either. In the case of $DyFe_3(BO_3)_4$, completely symmetric moments strongly depend on temperature in view of a more complex structure of energy levels, and thermal expansion anomalies can be observed. The calculated temperature dependences of completely symmetric moments of the Ho^{3+} ion in alumoborate $HoAl_3(BO_3)_4$ [17] predict thermal expansion anomalies at $T < 100$ K.

To our knowledge, thermal expansion has been measured by now only for $TmAl_3(BO_3)_4$ [9] (Fig. 6a); it was found that the crystal length along the c axis exhibits a nonlinear temperature dependence with a minimum near $T = 50$ K and a negative thermal expansion at low temperatures. Figure 6b shows the temperature dependences of variation of completely symmetric multipole moments $-\alpha_J\langle O_2^0\rangle$ and $-\beta_J\langle O_4^0\rangle$ and of the substantially smaller moment $-\beta_J\langle \Omega_4^3\rangle$ with coefficient 5. Generally speaking, the behavior of all three completely symmetric moments with their own coefficients ($A_{a,c}$, $B_{a,c}$, and $C_{a,c}$; see formulas (5) and (6)) is responsible for the observed thermal expansion anomalies or their absence at $T < 100$ K. It can be seen from Fig. 6b that the temperature variation of all three moments is in good agreement with the nonmonotonic experimental dependences of thermal expansion (Fig. 6a). The calculated temperature dependences of all moments display a peak near $T = 50$ K, after which the curves increase at different rates upon an increase in temperature in accordance with experiment.

Let us consider the temperature range $T < 100$ K, in which the phonon contribution can be assumed to be frozen out, and the observed anomalies are associated with the rare-earth contribution. Figure 7 illustrates the description of low-temperature anomalies in the thermal expansion taking into account only of the two most strongly varying moments ($-\alpha_J\langle O_2^0\rangle$ for $\Delta a/a$ and $-\beta_J\langle O_4^0\rangle$ for $\Delta c/c$). It can be seen that the inclusion of only one moment makes it possible to describe the experimental results quite satisfactorily. A more accurate description of the temperature variations of lattice parameters a and c for $TmAl_3(BO_3)_4$ can be obtained taking into account all three moments and selecting the coefficients in their linear combinations (formulas (5) and (6)). The expressions for coefficients A_a of $\alpha_J\langle O_2^0\rangle$ (formula (5)) and B_c of $\beta_J\langle O_4^0\rangle$ (formula (6)) for a trigonal lattice, which depend on magnetoelastic coefficients $B_{n0}^{\alpha m}$ and elastic constants $C_0^{\alpha k}$ (see [13] for notation), have the form

$$A_a = \frac{B_{20}^{\alpha 1}\left(C_0^{\alpha 2} + \frac{1}{\sqrt{2}}C_0^{\alpha 12}\right) - B_{20}^{\alpha 2}\left(\frac{1}{\sqrt{2}}C_0^{\alpha 1} + C_0^{\alpha 12}\right)}{\sqrt{3}(C_0^{\alpha 1}C_0^{\alpha 2} - (C_0^{\alpha 12})^2)}, \quad (10)$$

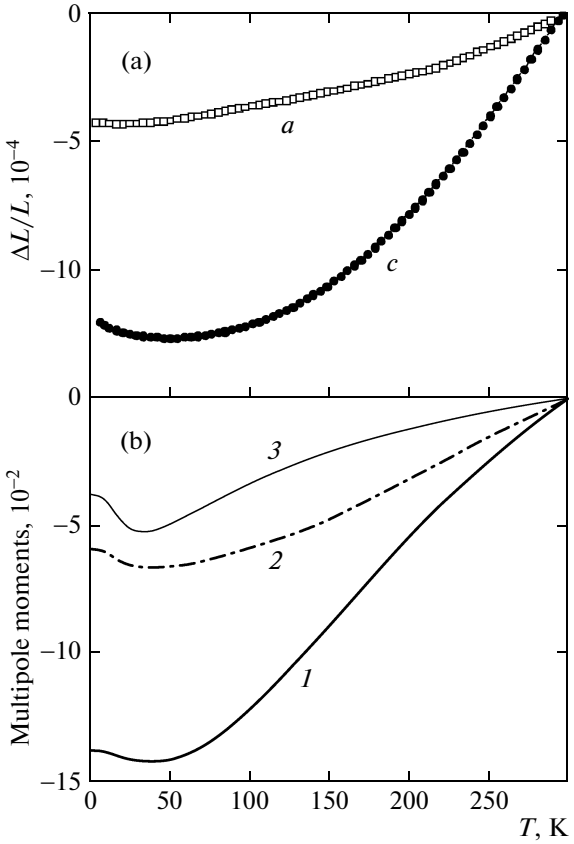

Fig. 6. (a) Experimental temperature dependences of variation of lattice parameters a and c of $TmAl_3(BO_3)_4$ [9]; (b) temperature dependences of completely symmetric multipole moments of Tm^{3+} ion in $TmAl_3(BO_3)_4$; $-\alpha_J(\langle O_2^0\rangle_T - \langle O_2^0\rangle_{T=300\text{ K}})$ (*1*), $-\beta_J(\langle O_4^0\rangle_T - \langle O_4^0\rangle_{T=300\text{ K}})$ (*2*), and $-5\beta_J(\langle \Omega_4^3\rangle_T - \langle \Omega_4^3\rangle_{T=300\text{ K}})$ (*3*).

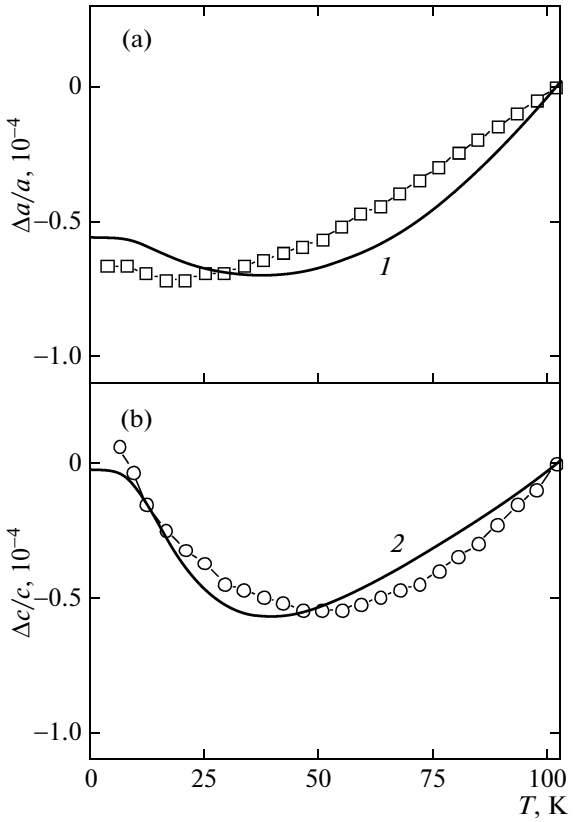

Fig. 7. Low-temperature dependences of variation of lattice parameters (a) $\Delta a/a$ and (b) $\Delta c/c$ of $TmAl_3(BO_3)_4$ [9] and variation of completely symmetric multipole moments of the Tm^{3+} ion taking into account resulting coefficients A_a and B_c: $-\alpha_J A_a(\langle O_2^0\rangle_T - \langle O_2^0\rangle_{T=100\text{ K}})$ (*1*), $-\beta_J B_c(\langle O_4^0\rangle_T - \langle O_4^0\rangle_{T=100\text{ K}})$ (*2*).

$$B_c = \frac{B_{40}^{\alpha 1}\left(C_0^{\alpha 2} - \frac{2}{\sqrt{2}}C_0^{\alpha 12}\right) + B_{40}^{\alpha 2}\left(\frac{2}{\sqrt{2}}C_0^{\alpha 1} - C_0^{\alpha 12}\right)}{\sqrt{3}(C_0^{\alpha 1}C_0^{\alpha 2} - (C_0^{\alpha 12})^2)}. \quad (11)$$

Information on the magnetoelastic coefficients and elastic constants of $TmAl_3(BO_3)_4$ is not available. However, an analysis of the experimental dependences of thermal expansion makes it possible to estimate coefficients A_a and B_c from low-temperature regions ($T < 100$ K) $A_a = 3.45 \times 10^{-3}$ and $B_c = 7.3 \times 10^{-3}$. Thus, information on the thermal expansion can serve as a reference point in the search for the values of magnetoelastic coefficients and elastic constants.

It should be noted that CF parameters (7), which have made it possible to successfully describe the magnetoelastic effects in $TmAl_3(BO_3)_4$ [9], were determined from the magnetic characteristics measured by us and from our spectroscopic data.

5. CONCLUSIONS

The magnetic, magnetoelastic, and spectroscopic properties of alumoborate $TmAl_3(BO_3)_4$ have been analyzed. The resultant CF parameters make it possible to interpret all measured characteristics of $TmAl_3(BO_3)_4$ and all observed peculiarities.

The temperature and field dependences of magnetization $M_{c,\perp c}(T, B)$ have been described. It is found that the low-temperature region ($T < 50$ K) of the $M_c(T)$ curve measured in our experiments at $B = 0.1$ T differs from that of the $\chi_c(T)$ curve from [9, 11]. Our calculations of the field and temperature dependences of multipole moments of the Tm^{3+} ion in $TmAl_3(BO_3)_4$ have shown that in conformity with experiment, the variation of the crystal length along the a axis is nonlinear when the field is directed along the a axis. In this case, $\alpha_J\langle O_2^2\rangle$ is the largest moment for which the temperature and field dependences correctly reproduce the temperature and field dependences of magnetostriction. In the low-temperature range, thermal

expansion anomalies associated with the change in the electron configuration of the 4*f* shell of the R ion are observed and described. The coefficients determining the magnetostriction and thermal expansion anomalies are estimated from a comparison of the results of calculations and experimental data.

ACKNOWLEDGMENTS

This study was supported financially by the Russian Foundation for Basic Research (project no. 13-02-12442ofi_m2) and (K.N.B.) by the grant no. MK-1700.2013.2 from the President of the Russian Federation.

REFERENCES

1. A. K. Zvezdin, S. S. Krotov, A. M. Kadomtseva, G. P. Vorob'ev, Yu. F. Popov, A. P. Pyatakov, L. N. Bezmaternykh, and E. A. Popova, JETP Lett. **81** (6), 272 (2005).
2. E. A. Popova, D. V. Volkov, A. N. Vasiliev, A. A. Demidov, N. P. Kolmakova, I. A. Gudim, L. N. Bezmaternykh, N. Tristan, Yu. Skourski, B. Büchner, C. Hess, and R. Klingeler, Phys. Rev. B: Condens. Matter **75**, 224413 (2007).
3. E. A. Popova, N. I. Leonyuk, M. N. Popova, E. P. Chukalina, K. N. Boldyrev, N. Tristan, R. Klingeler, and B. Büchner, Phys. Rev. B: Condens. Matter **76**, 054446 (2007).
4. J. E. Hamann-Borrero, S. Partzsch, S. Valencia, C. Mazzoli, J. Herrero-Martin, R. Feyerherm, E. Dudzik, C. Hess, A. Vasiliev, L. Bezmaternykh, B. Büchner, and J. Geck, Phys. Rev. Lett. **109**, 267202 (2012).
5. N. V. Volkov, I. A. Gudim, E. V. Eremin, A. I. Begunov, A. A. Demidov, and K. N. Boldyrev, JETP Lett. **99** (2), 67 (2014).
6. T. Usui, Y. Tanaka, H. Nakajima, M. Taguchi, A. Chainani, M. Oura, S. Shin, N. Katayama, H. Sawa, Y. Wakabayashi, and T. Kimura, Nat. Mater. **13** (6), 611 (2014).
7. A. M. Kadomtseva, Yu. F. Popov, G. P. Vorob'ev, A. P. Pyatakov, S. S. Krotov, K. I. Kamilov, V. Yu. Ivanov, A. A. Mukhin, A. K. Zvezdin, A. M. Kuz'menko, L. N. Bezmaternykh, I. A. Gudim, and V. L. Temerov, Low Temp. Phys. **36** (6), 511 (2010).
8. A. I. Popov, D. I. Plokhov, A. K. Zvezdin, Phys. Rev. B: Condens. Matter **87**, 024413 (2013).
9. R. P. Chaudhury, B. Lorenz, Y. Y. Sun, L. N. Bezmaternykh, V. L. Temerov, and C. W. Chu, Phys. Rev. B: Condens. Matter **81**, 220402 (2010).
10. K.-C. Liang, R. P. Chaudhury, B. Lorenz, Y. Y. Sun, L. N. Bezmaternykh, V. L. Temerov, and C. W. Chu, Phys. Rev. B: Condens. Matter **83**, 180417(R) (2011).
11. K.-C. Liang, R. P. Chaudhury, B. Lorenz, Y. Y. Sun, L. N. Bezmaternykh, I. A. Gudim, V. L. Temerov, and C. W. Chu, J. Phys.: Conf. Ser. **400**, 032046 (2012).
12. A. I. Begunov, A. A. Demidov, I. A. Gudim, and E. V. Eremin, JETP Lett. **97** (9), 528 (2013).
13. A. A. Demidov, N. P. Kolmakova, L. V. Takunov, and D. V. Volkov, Physica B (Amsterdam) **398**, 78 (2007).
14. D. V. Volkov, A. A. Demidov, N. P. Kolmakova, and L. V. Takunov, Phys. Solid State **50** (9), 1677 (2008).
15. A. A. Demidov, N. P. Kolmakova, D. V. Volkov, and A. N. Vasiliev, Physica B (Amsterdam) **404**, 213 (2009).
16. D. V. Volkov and A. A. Demidov, *Proceedings of the 35th Workshop on Low Temperature Physics, Institute of Problems of Chemical Physics of the Russian Academy of Sciences, Chernogolovka, Moscow oblast, Russia, September 29–October 2, 2009* (Chernogolovka, 2009), p. 158.
17. A. I. Begunov, D. V. Volkov, and A. A. Demidov, Phys. Solid State **56** (3), 511 (2014).
18. N. P. Kolmakova, R. Z. Levitin, V. N. Orlov, and N. F. Vedernikov, J. Magn. Magn. Mater. **87**, 218 (1990).
19. N. P. Kolmakova, L. V. Takunov, and O. A. Shishkina, Physica B (Amsterdam) **352**, 259 (2004).
20. L. N. Bezmaternykh, V. L. Temerov, I. A. Gudim, and N. A. Stolbovaya, Crystallogr. Rep. **50** (Suppl. 1), 97 (2005).
21. V. L. Temerov, A. E. Sokolov, A. L. Sukhachev, A. F. Bovina, I. S. Edel'man, and A. V. Malakhovskii, Crystallogr. Rep. **53** (7), 1157 (2008).
22. Z. A. Kazei, N. P. Kolmakova, and O. A. Shishkina, Physica B (Amsterdam) **245**, 164 (1998).
23. I. Kebaili, M. Dammak, and E. Cavalli, J. Luminnescence **131**, 2010 (2011).
24. I. Couwenberg, K. Binnemans, H. De Leebeeck, and C. Görller-Walrand, J. Alloys Comp. **274**, 157 (1998).
25. A. Kirste, M. von Ortenberg, A. A. Demidov, Z. A. Kazei, N. P. Kolmakova, V. V. Platonov, A. A. Sidorenko, and O. M. Tatsenko, Physica B (Amsterdam) **336**, 335 (2003).
26. A. A. Demidov, Candidate's Dissertation in Mathematical Physics (Moscow State University, Moscow, 2004).
27. B. Lüthi and H. R. Ott, Solid State Commun. **33**, 717 (1980).
28. N. P. Kolmakova, R. Z. Levitin, and V. N. Orlov, Phys. Status Solidi A **115**, K87 (1989).

Translated by N. Wadhwa